The Influence of Non-planar (Spatial) Links in the Static Characteristics Behavior of Planar Parallel Manipulator

Ganesh M.[1], Karthikeyan R.[2], Venkitachalam P.[3], Guruguhan G.[4], S. Shrinithi[5], Kannan S.[6], Anjan Kumar Dash[7]

[1,2,3,4,5,7] School of Mechanical Engineering. SASTRA University, India
[6] School of Electrical and Electronics Engineering. SASTRA University, India

ABSTRACT

Conventional planar manipulators have all their links in a single plane. Increasing payload at the end-effecter/mobile platform can induce high stress in the links due to cantilever nature of links. Thus it limits the total vertical load that can be applied on the mobile platform. In contrast to the links in conventional planar parallel mechanisms, non-planar links are proposed in this paper, i.e., links are made inclined to the horizontal plane and non planar legs are constructed. Although the links are made non-planar, the rotary (or prismatic) joints axes remain perpendicular (or parallel) to the plane of the base platform, which retains the planar motion of the end-effecter. For studying the application of such non planar links in planar manipulators, new models of inertia, stiffness and leg dynamics have to be developed. In this article, these models are developed and with the developed models, the static analysis is done on the planar manipulators with non-planar links and the performance is compared with the corresponding conventional planar manipulators.

Corresponding Author:

Ganesh M.,
School of Mechanical Engineering,
SASTRA University,
Thanjavur–613 402, India.
Email: ganeshm@mech.sastra.edu

1.   INTRODUCTION

Parallel robots have been under intensive study for over more than one decade. It is well known that parallel kinematic structures offer advantages such as high accuracy, payload-to-weight ratio, high natural frequencies and rigidity compared to serial manipulators. Of the parallel manipulators, 3-dof planar parallel manipulators are widely used as Parallel Kinematic Machine. So it has attracted many researchers to study on its workspace [1],[2], direct kinematics[3] singularity Analysis[4],[5] and optimal design[6],[7].

Planar manipulators find its application in fast positioning or assembly operations. Such applications make use of the high speed capability with minimum positioning error, large stiffness [8],[9] and low inertia[10] of parallel planar manipulators. Parallel Planar manipulators belonging to such category is shown in Figure 1.

In applications where there is a heavy load on the platform, the vertical load will create a cantilever action on each of the links. Thus there is a chance that it may limit the total vertical load that can be applied.In this paper, planar manipulator with non-planar links is proposed. For a manipulator with non-planar links, links are not in single plane. The links are elevated and distance between base platform and top platform is raised.In this proposed design, each link is inclined with respect to the horizontal plane and it is expected to carry a higher payload and decrease the cantilever nature of the links.
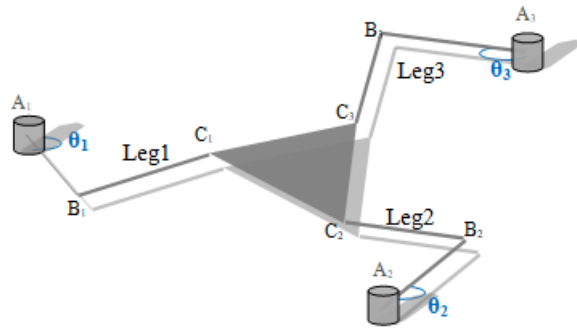
Figure 1a. A planar 3-RRR Manipulator

Figure 1b. A planar robot with 3-PRR configuration [11]

In nature also, this design is more closely oriented towards the behavior of many living entities. The following illustrations depict the usage of inclined links. Figure 2 shows the usage of inclined links for carrying the heavy loads. The inclined leg of the insect comes handy to maneuver the load of the insect body. In another case, inclined links of the hand is used to transmit high forces and accurate positioning without causing strain to the links.

Figure 2. The usage of inclined links

In practice, the load bearing capability can be significantly improved with inclined links which can be appreciated from the above figures. It is also obvious that non-planar links are going to influence many other characteristics. Out of them, the following features of the manipulator –*moment of inertia, stiffness, workspace, inertia forces* and *mass in motion* are addressed in this article. The existing mathematical models for the above parameters are rendered to reflect the changes in the model. In this article, the authors will be referring to the manipulator with Non-Planar Link Arrangement as 'NPLA manipulator' throughout the paper, for simple usage of language.

Assuming cylindrical links (with circular cross section) for the manipulator legs, *moment of inertia* and *Mass moment of inertia* of the links are determined. Conventional *Stiffness analysis* is usually done by Jacobian method [12] which presumes the links as rigid elements and only active joint stiffness is considered [13]. In Matrix structural analysis [14], the links are flexible and the passive joint stiffness is also included. In this article, the matrix structural approach is followed to study the proposed manipulator design with non-planar links.

While designing a parallel manipulator for a particular application, the *singularity-free workspace area* is of major concern. Voids inside the workspace fall under the category of *Type-I singularities.* It can be shown that the *Type II singularities* occur when the wrenches are parallel or intersecting at one common point [15]. Since the wrenches or the lines associated with the distal links, behave identical to the conventional manipulator, this paper will be addressing only Type-I singularities while optimizing the design parameters.

The design parameters for a specific manipulator are optimized. The main design parameter of interest here is the inclination angle. Although it can be easily understood that increasing the inclination angle improves the load bearing capability and stiffness, but it may affect the *workspace* or *mass of manipulator* in motion. It will be of the readers' interest to know the appropriate inclination angle which does not compromise any significant feature of the manipulator. In this article, the manipulator is optimized to have low mass in motion, high stiffness and maximum force transmission in a prescribed void-free workspace area.

The new models for the above mentioned specific kinematic parameters are obtained with generalized RR configuration and it is to be noted that this configuration features is in each leg of the manipulator. A 3-RRR NPLA manipulator is taken as case study to discuss the results of the analysis. It is shown that the models can also be developed for other manipulators (with non-planar links) such as 3-PRR and 3 –RPR, following the methodology described.

The proposed design is introduced in section 2 with illustrations. In section 3, the rotational inertia (mass moment of inertia) for the inclined links is obtained. Assuming the links to be flexible, computation of the stiffness matrix for RR configuration is done. These computations are shown in comparison with the conventional manipulator. For NPLA 3-RRR, Jacobian based static force analysis and the results of stiffness analysis is discussed in section 4. Finally an optimized inclination angle is obtained for the Non-planar (spatial) links of 3-RRR.

2.   PROPOSED DESIGN OF NON-PLANAR LINKS

In the proposed design, the links are not in a single horizontal plane. The links are made non-planar by making it inclined about X-Y plane. This results in an increased distance between the base platform and mobile platform. The principle idea of elevating one of the links is shown in Figure 3. The first link L1 of this mechanism is rotated by θ_1 degrees about Z-axis. By this L1 is shifted to Li′ in XY plane as shown in Figure 3. It is again rotated δ_1 degrees, but this time it is about Y axis of L1′. Thus L1′ is shifted to L1″. The same procedure is repeated for the other links of the leg. For symmetry purpose δ is kept constant for all the links. Depending on the rotation of links about its Y-axis (δ_1), the height of the top platform and the radius of the top platform can be varied. This is decided based on requirement of kinematics parameters such as workspace, stiffness and force transmission.
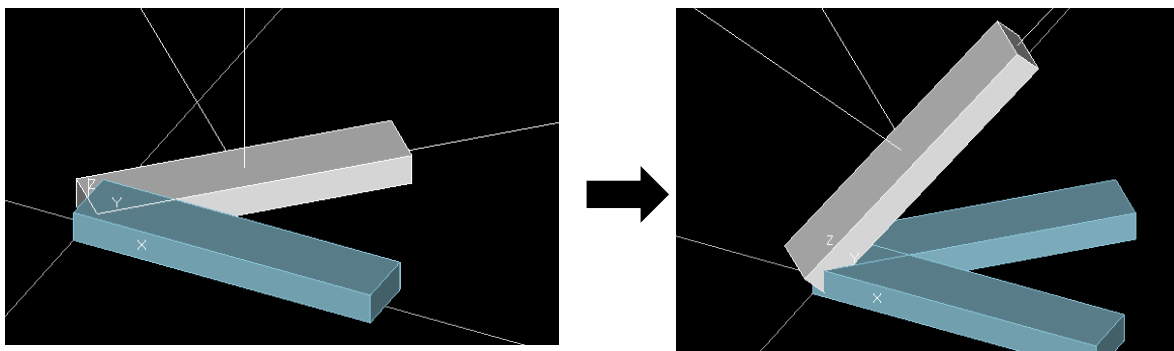
Figure 3. Principle of Inclination

If L_1'' is projected unto the base plane, its length/magnitude will be $L_1''\cos\delta_1$ as shown in Figure.3. If the link L_1'' is rotated any further about Z axis, *i.e.* with any change in the value of θ_1, the distance ($L_1''\cos\delta_1$) remains unchanged. Hence, the kinematics for this model will be realized on a projected horizontal plane with the link lengths being the horizontal distance between any two joints.

The above mentioned procedure is applied for all the legs. For the proposed NPL arrangement, although the links are made inclined to the horizontal plane, the rotary (or prismatic) joints axes remain perpendicular (or parallel as the case may be) to the plane of the base platform, which retains the planar motion of the end-effecter. The conceived proposal for the following configurations 3 RRR, 3- PRR and 3-RRP is illustrated in Table 1.

Table 1. Shows the Schematic of NPLA in Individual Leg of Planar Manipulators

Planar Manipulators	Single Leg - Conventional	Single leg- NPLA Arrangement
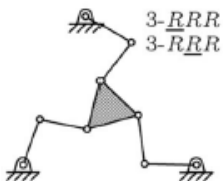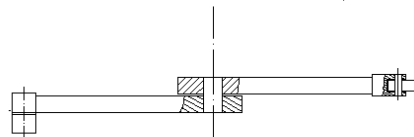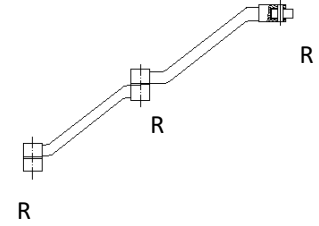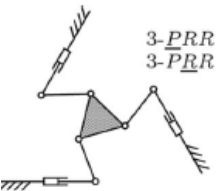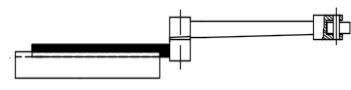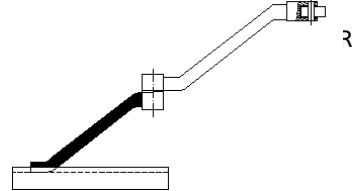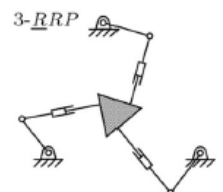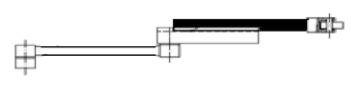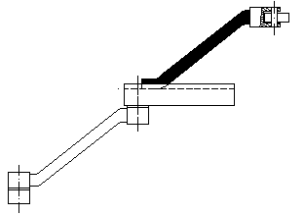
3.   RESEARCH METHOD

New mathematical models are required for studying the influence of the inclination angle in relation to the following parameters- moment of inertia, stiffness, static forces, mass in motion and workspace.

3.1. Formulation of Inertia Tensor

Assuming cylindrical links (with circular cross section) for the manipulator legs, Moment of Inertia(MOI) and Mass moment of inertia for the links are determined. Let the inclined link be of radius R and length L in XZ- plane. In order to determine the moment of inertia (second moment of area) about the Z-axis as shown in Figure 4, the cross section area of the inclined link in the X-Y plane is considered. The cross section area is an ellipse with minor diameter equals R and major diameter is R / cos δ, as the link is inclined about an angle δ.
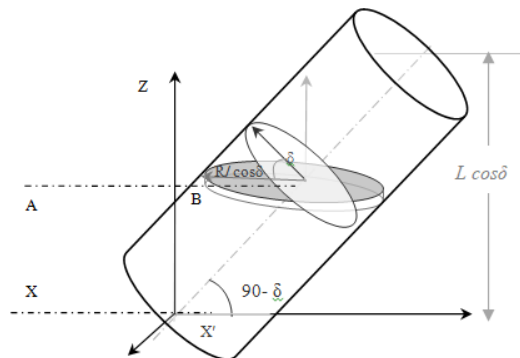
Figure 4. A link is shown in XZ plane with an inclination of $\delta°$ about X axis. The link has an elliptical cross section in XY plane.This elliptical cross section area is used for computing the moment of inertia

Assuming the link as a 3D spring model, the compliance matrix for the link element is (1)

$$C_M = \frac{1}{E} \begin{bmatrix} L/A & 0 & 0 & 0 & 0 & 0 \\ 0 & 1/3I_z L & 0 & 0 & 0 & -1/2I_z \\ 0 & 0 & 1/3I_y.L & 0 & -1/2I_y & 0 \\ 0 & 0 & 0 & \frac{E.L}{G.J} & 0 & 0 \\ 0 & 0 & -1/2I_y & 0 & L/I_y & 0 \\ 0 & 1/2I_z & 0 & 0 & 0 & L/I_z \end{bmatrix} \tag{1}$$

In the matrix elements, cross section area A and inertia I will be corresponding to the elliptical cross section and they are given by equation (2) and (3) respectively

Area of cross section $A = \pi r \dfrac{r}{\cos\delta}$ (2)

Polar moment of inertia $I_z = I_y + I_x = \pi \dfrac{r^4}{4}\left[\left(\dfrac{1}{\cos\delta}\right) + \left(\dfrac{1}{\cos\delta}\right)^3\right]$ (3)

Due to the presence of $\cos\delta$ term in equation 2 and 3, moment of inertia increases nonlinearly with δ. With the rise in moment of inertia, the compliance of the links is very much reduced in comparison to the links of planar legs.

Mass Moment of inertia

The mass moment of inertia of the links is very much reduced as the cross section area about the vertical axis has changed. This will influence the accurate modeling of leg dynamics. The moment of inertia of the thin elliptical disc shown in Figure 5 about the axis AB is given as (4)

$$I_{AB} = \left(\frac{1}{4}\right) M a^2 \tag{4}$$

where $a = R/\cos\delta$
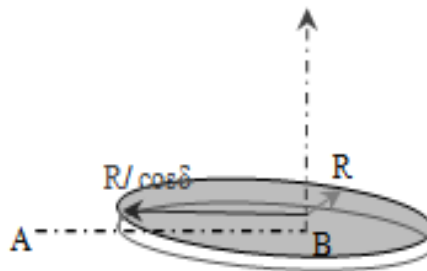
Figure 5. Thin elliptical disc region of inclined link

To calculate the Moment of Inertia about X-axis passing through one end of the link, parallel axis theorem is applied (5-6)

$$I_{xx} = I_{AB} + dm.x^2$$

Where $dm = \left(\dfrac{M}{L\cos\delta}\right) dx$ (5)

$$I_{xx} = \left(\frac{1}{4}\right)\frac{MR^2}{\cos^2\delta} + \left(\frac{1}{3}\right)ML^2\cos^2\delta$$

(6)

Similar to the bending moment inertia as discussed above, the presence of δ term significantly influences the mass moment of inertia. By analyzing Eqn 6, it can be understood that the value of the first term raises the inertia value whereas the second term lowers the inertia value, due to the occurrence of sinδ term. Since the length to diameter ratio is significantly high, the influence of the first term is very less and overall inertia factor is reduced. It can be noted that the mass moment of inertia is the rotational inertia, which when reduced is much favorable for the rotary motor actuation.

3.2. Stiffness modeling of RR configuration

As mentioned in the introduction section, the matrix structural approach is adopted to study the stiffness of non-planar links. With this modeling approach, the inertia parameters modified in the above section are substituted in the compliance matrix of link elements. The influence is studied in comparison with the planar parallel manipulator.

The following methodology as proposed by Nagai and Liu [17] determines the stiffness model for a parallel mechanism.In this method the parallel mechanism is sub-divided into kinematic chains representing each leg. Each chain is further divided into mechanical modules in which the module represents a joint and its associated link[a]. The stiffness of the kinematic chain is obtained by iteratively adding each mechanical module. Step by step procedure is given below and illustrated in Figure 6.

a. **Step 1** Links are assumed flexible. A 2D or 3D spring model is used to determine the compliance for the link.
b. **Step 2** Joint compliance is determined by the conventional method.
c. The link compliance and the joint compliance together represent the compliance of a mechanical module.
d. **Step 3** The compliance for the mechanical module is transformed to global reference by suitable transformations.
e. **Step 4** Steps 1to 3 are repeated for each module. (Each joint and its associate link)
f. **Step 5** The compliance matrix hence obtained for each module is cumulatively added to give the total compliance of the kinematic chain. The inverse of the total compliance gives the stiffness of each chain.

[a] For a nth joint, n-1th link denotes the associated kinematic chain.
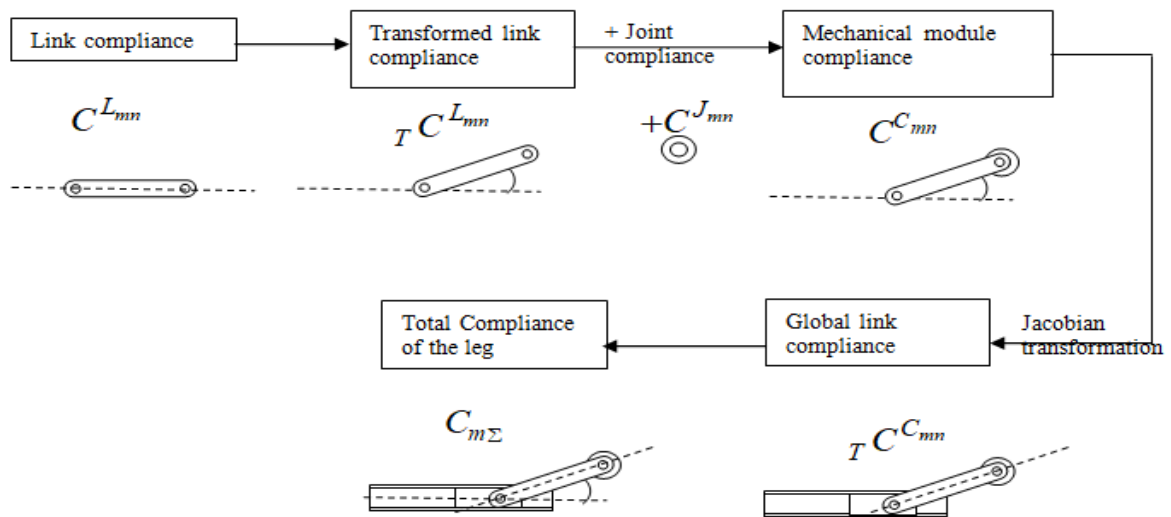
Figure 6. shows the flow chart of methodology in determining the stiffness of a kinematic chain

The stiffness analysis is carried for RR configuration of the manipulator and extended for the other legs. The study is done in comparison with the planar links. For planar links, the modeling is based on 2 dimensional approach, whereas for non-planar links the modeling is by a 3- dimensional approach. *Stiffness*

model for RR configuration-First Mechanical module (1st joint and its previous link) Since the first joint is an active joint, the compliance for the joint C^{J11} is taken as $diag(0,0,S_{11}^{-1})$. The active joint with first link (Leg-1) conventional design and modified design as shown in Figures 7a and 7b. Considering the first link of Leg-1

$$C^{C11} =_T C^{L10} + C^{J11} \tag{7a}$$

where C^{C11} denotes the cumulative compliance (1st joint and 0th transformed link). Refer appendix A for the notation
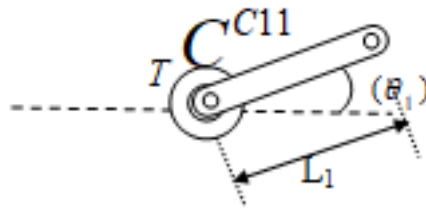
Figure 7a. The active joint with first link (Leg-1)-Conventional design

Considering the first link of Leg-1

$$C^{C11} =_T C^{L10} + C^{J11} \tag{7b}$$
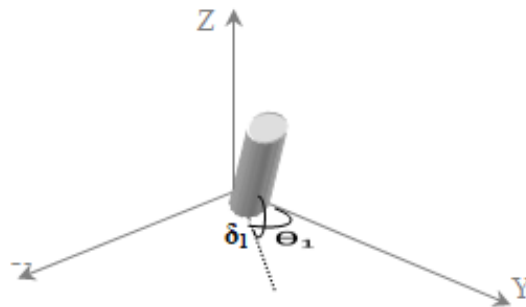
Figure 7b. The active joint with first link (Leg-1) - Modified design

The transformed compliance $_T C^{C11}$ for this mechanical module (1st joint and previous link together) is computed by equation (8) as shown below

$$_T C^{C11} = \begin{bmatrix} {}^B R_{ij} & {}^B R_{ij}[{}^{ij}P_T] \\ 0 & 1 \end{bmatrix} C^{C11} \begin{bmatrix} {}^B R_{ij} & 0 \\ {}^B R_{ij}[{}^{ij}P_T] & 1 \end{bmatrix} \tag{8a}$$

$$_T C^{C11} = \begin{bmatrix} {}^B R_{ij} & {}^B R_{ij}[{}^{ij}P_T] \\ 0 & {}^B R_{ij} \end{bmatrix} C^{C11} \begin{bmatrix} {}^B R_{ij} & 0 \\ {}^B R_{ij}[{}^{ij}P_T] & {}^B R_{ij} \end{bmatrix} \tag{8b}$$

Second Mechanical module (2nd joint and its previous 1st link)

Links are assumed not to be rigid. So compliance for the links is obtained by materials science – Structural analysis approach. A 2D spring model is assumed for this approach equation (9a) represents the compliance components

$$_L C = \frac{1}{E} \begin{bmatrix} \dfrac{L}{A} & 0 & 0 \\ 0 & \dfrac{L^3}{3I} & \dfrac{L^2}{-2I} \\ 0 & \dfrac{L^2}{-2I} & \dfrac{L}{I} \end{bmatrix} \tag{9a}$$

A 3D spring model is assumed for the modified design to incorporate all deflections along and around X, Y and Z axes of the Cartesian space in equation 9b. The compliance matrix is given by equation (1) (*Section 3*). The expressions of the compliance matrix elements are modified and they are illustrated in section 3.1. This makes an impact in the stiffness matrix calculations

$$_L C = C_M \tag{9b}$$

The compliance matrix in equation. (9) represents the local stiffness matrix. It has to be transformed globally by rotational transformation as shown below in equation. (10).

$$R_1 = \begin{bmatrix} C\theta_1 & -S\theta_1 & 0 \\ S\theta_1 & C\theta_1 & 0 \\ 0 & 0 & 1 \end{bmatrix} \tag{10a}$$

Rotation about Z axis

$$R_1 = \begin{bmatrix} C\theta_1 & -S\theta_1 & 0 \\ S\theta_1 & C\theta_1 & 0 \\ 0 & 0 & 1 \end{bmatrix} \times \begin{bmatrix} C\delta_1 & 0 & S\delta_1 \\ 0 & 1 & 0 \\ -S\delta_1 & 0 & C\delta_1 \end{bmatrix} \tag{10b}$$

Rotation about Z axis Rotation about Y axis

For the conventional planar manipulator, the following equation (11a) determines the transformed link compliance.

$$_T C^{L11} = R_1 \times {}_L C \times R_1^{T} \tag{11a}$$

For the modified NPLA design, the following equation (11b) determines the transformed link compliance. equation (9b) and (10b) are substituted in equation (11b)

$$_T C^{L11} = \begin{bmatrix} R_1 & 0 \\ 0 & R_1 \end{bmatrix} \times {}_L C \times \begin{bmatrix} R_1^{T} & 0 \\ 0 & R_1^{T} \end{bmatrix} \tag{11b}$$

The total stiffness C^{C12} is combination of 2nd joint stiffness and 1st link stiffness. Since the second joint is a passive joint, its compliance C^{J12} is neglected. Thus (12),

$$C^{C12} = {}_T C^{L11} + C^{J12} \tag{12}$$

Applying the same method of transformation as done in equation (8), the following equation (13) is obtained

$$_TC^{C12} = \begin{bmatrix} ^BR_{ij} & ^BR_{ij}[^{ij}P_T] \\ 0 & 1 \end{bmatrix} C^{C12} \begin{bmatrix} ^BR_{ij} & 0 \\ ^BR_{ij}[^{ij}P_T] & 1 \end{bmatrix} \tag{13}$$

Third Mechanical module (3rd joint and its previous 2nd link)

The transformed link compliance is repeated for second link of leg1. The same steps are repeated. The generalized link length L will be equivalent to l_d in the compliance matrix. The rotation matrix R_2 will have θ_2. For symmetry purpose δ_2 is taken δ_1 Figure 8.
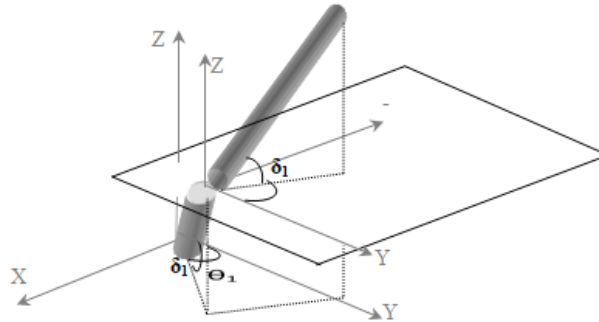
Figure 8. Third Mechanical module of modified design

Now, considering the third joint as passive, the following equation (14) is obtained.

$$C^{C13} = {}_TC^{L12} + C^{J13} \tag{14}$$

Repeating the same transformation used in equation (8) as follow (15)

$$_TC^{C13} = \begin{bmatrix} ^BR_{ij}\,^BR_{ij}[^{ij}P_T] \\ 0 & 1 \end{bmatrix} C^{C13} \begin{bmatrix} ^BR_{ij} & 0 \\ ^BR_{ij}[^{ij}P_T]1 \end{bmatrix} \tag{15}$$

Adding equations (8), (13) and (15), the total stiffness of a chain of RRR is determined as given below (16).

$$C_{1\Sigma} = {}_TC^{C11} + {}_TC^{C12} + {}_TC^{C13} \tag{16}$$

Taking inverse of equation (16), the stiffness of one leg is obtained.

3.3. A case study- 3-RRR manipulator

An initial prototype of 3-RRR planar manipulator is fabricated for with non-planar links as shown Figure 9. In order to have a simplified kinematics, different geometric parameters chosen are as follows. The kinematics is decided for a link length of 100 mm and mobile platform size of 180 mm. In such case, the actual link length will be L = *100/cosδ₁*

The height of the mobile platform from the base is chosen as 250 mm. So each link has to be elevated 125 mm, if the expected projection to be same for each of the links. Hence the angle of elevation becomes

tan δ₁ = 125/100
δ₁= 51.32°

For ease in manufacturing, δ is taken as 50°
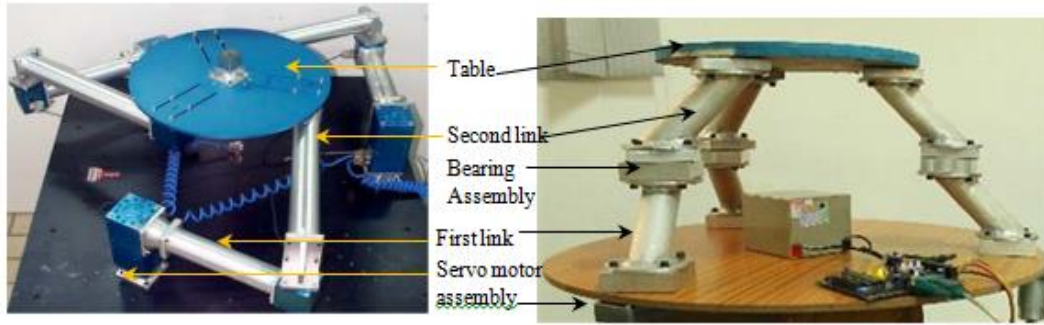
Figure 9. Conventional 3-RRR planar robot[15] and the proposed manipulator prototype[19]

3.3.1 Jacobian Analysis of 3-RRR NPLA Manipulator

Using the principle of Screw theory, force jacobian is obtained for 3-RRR planar manipulator with the non-planar links. This jacobian is required for analyzing the static forces in comparison with the conventional planar manipulator. Twist annihilators are used for elimination of the idle variables in the kinematic relations[18]. The End-effectors twist is linearly related to the joint-rate vector $\dot{\theta}$, by (17)

$$J\dot{\theta} = t$$

where J is the screw based *Jacobian matrix,* of the manipulator under study.

$$J \equiv \begin{bmatrix} e_1 & e_2 & e_3 \\ e_1 \times r_1 & e_2 \times r_2 & e_3 \times r_3 \end{bmatrix}, \dot{\theta} \equiv \begin{bmatrix} \dot{\theta}_{i_1} \\ \dot{\theta}_{i_2} \\ \dot{\theta}_{i_3} \end{bmatrix}, t \equiv \begin{bmatrix} w \\ P \end{bmatrix} \tag{17}$$

where r_i is the vector directed from i^{th} joint to end –effector shown as in Figure 10, and P is the position vector of the end–effecter.
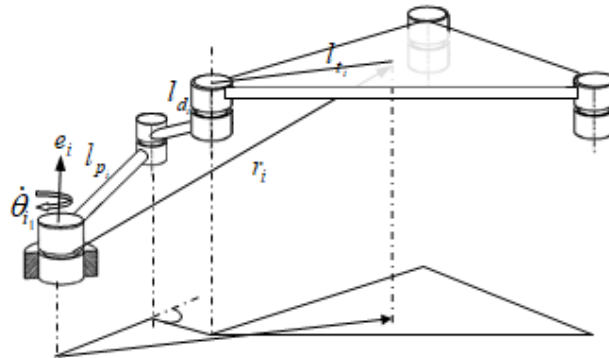
Figure 10. Single leg of a non-planar 3-RRR

Solving by Gaussian elimination, we get the expression of active joint for a single leg I (18)

$$[(x_1 - x_2)(y_3 - y_2) - (y_1 - y_2)(x_3 - x_2)]\dot{\theta}_{l_1}$$

$$= [(x_3 - x_2) \quad (y_3 - y_2) \quad (x_3 - x_2)y_2 - x_2(y_3 - y_2)] \begin{bmatrix} x_p \\ y_p \\ \dot{\phi} \end{bmatrix} \tag{18}$$

Where, $x_1 = l_{p_1} C_{1_1} + l_{d_1} C_{12_1} + l_{t_1} C_{123_1}$; $y_1 = l_{p_1} S_{1_1} + l_{d_1} S_{12_1} + l_{t_1} S_{123_1}$;

$\qquad x_2 = l_{d_1} C_{12_1} + l_{t_1} C_{123_1}$; $\qquad y_2 = l_{d_1} S_{12_1} + l_{t_1} S_{123_1}$;

$\qquad x_3 = l_{t_1} C_{123_1}$; $\qquad\qquad y_3 = l_{t_1} S_{123_1}$;

(The angle notations is briefed below)

$$C_{12_1} \rightarrow Cos(\theta_1 + \theta_2)\, for\, leg\, 1$$
$$S_{12_1} \rightarrow Sin(\theta_1 + \theta_2)\, for\, leg\, 1$$

Substituting the above set of equations. in equation 18, we get (19)

$$l_{p_1} l_{d_1} \left[C_{1_1} S_{12_1} - S_{1_1} C_{12_1} \right] \dot{\theta}_{1_1} = \left[l_{d_1} C_{12_1} \quad l_{d_1} S_{12_1} \quad l_{d_1} C_{12_1}(l_{d_1} S_{12_1} + l_{t_1} S_{123_1}) - l_{d_1} S_{12_1}(l_{d_1} C_{12_1} + l_{t_1} C_{123_1}) \right] \begin{bmatrix} x_p \\ y_p \\ \dot{\phi} \end{bmatrix} \qquad (19)$$

Similarly, deriving for all the three legs, and representing the three scalars in matrix form, we get $|A|\dot{\theta} = |B|\dot{q}$

For planar manipulator $\qquad\qquad$ **non-planar manipulator**

$$J = A^{-1}B \equiv \begin{bmatrix} \dfrac{C_{12_1}}{l_{p_1} S_{2_1}} & \dfrac{S_{12_1}}{l_{p_1} S_{2_1}} & \dfrac{l_{t_1} S_{3_1}}{l_{p_1} S_{2_1}} \\[2mm] \dfrac{C_{12_2}}{l_{p_2} S_{2_2}} & \dfrac{S_{12_2}}{l_{p_2} S_{2_2}} & \dfrac{l_{t_2} S_{3_2}}{l_{p_2} S_{2_2}} \\[2mm] \dfrac{C_{12_3}}{l_{p_3} S_{2_3}} & \dfrac{S_{12_3}}{l_{p_3} S_{2_3}} & \dfrac{l_{t_3} S_{3_3}}{l_{p_3} S_{2_3}} \end{bmatrix} \quad J = \begin{bmatrix} \dfrac{C_{12_1}}{(l_{p_1}\cos\delta)S_{2_1}} & \dfrac{S_{12_1}}{(l_{p_1}\cos\delta)S_{2_1}} & \dfrac{l_{t_1} S_{3_1}}{(l_{p_1}\cos\delta)S_{2_1}} \\[2mm] \dfrac{C_{12_2}}{(l_{p_2}\cos\delta)S_{2_2}} & \dfrac{S_{12_2}}{(l_{p_2}\cos\delta)S_{2_2}} & \dfrac{l_{t_2} S_{3_2}}{(l_{p_2}\cos\delta)S_{2_2}} \\[2mm] \dfrac{C_{12_3}}{(l_{p_3}\cos\delta)S_{2_3}} & \dfrac{S_{12_3}}{(l_{p_3}\cos\delta)S_{2_3}} & \dfrac{l_{t_3} S_{3_3}}{(l_{p_3}\cos\delta)S_{2_3}} \end{bmatrix}$$

3.3.2 Design Optimization

It can be understood that increasing the inclination angle improves the load bearing capability and stiffnes, but it may affect the *workspace* or *mass of manipulator* in motion. For example, when it is 90° with respect to the horizontal plane, a maximal payload can be achieved but the workspace becomes zero. Hence, it will be of the readers' interest to know the appropriate inclination angle which does not compromise any significant feature of the manipulator.

For optimization, a desirable workspace provided by the user is taken as a constraint. The stiffness along the Z axis and the force transmission in X-Y plane is maximized in the desirable workspace area. Hence the objective of optimization would be to minimize the mass in motion while maximizing the stiffness and force transmission of the parallel manipulator. The objectives are given below in brief.

a.   Mass of the manipulator = mass of 6 links + mass of the platform (20)

$$M_{RRR} = 3 \times \pi r_c^2 l_p \vartheta + 3 \times \pi r_c^2 l_d \vartheta + \pi r_{top}^2 t \vartheta \qquad (20)$$

where ϑ is the density of the material. For steel, the value is 7850 kg/m³ and for aluminium it is 2700 kg/m³

$\qquad$ r_c is the radius of link's circular cross section
$\qquad$ r_{top} is the radius of the top platform
$\qquad$ t is the thickness of the top platform

b.   The force components f_x and f_y acting at the end-effector can be solved from the force Jacobian obtained in S*ection 3.3.1*. The static force expression is obtained from the Jacobian matrix, because the force Jacobian is same as velocity Jacobian in case of 3-RRR planar manipulator [20]. Hence the end effecter output forces are directly obtained from the force Jacobian matrix and input torquesAssuming unit torque provided at the actuators, the force components are given below (21)

$$f_x = \frac{\cos(\theta_{2_1})}{l_p \times \cos\delta \times \sin(\theta_2 - \theta_1)_1} + \frac{\cos(\theta_{2_2})}{l_p \times \cos\delta \times \sin(\theta_2 - \theta_1)_2} + \frac{\cos(\theta_{2_3})}{l_p \times \cos\delta \times \sin(\theta_2 - \theta_1)_3}$$

(21)

$$f_y = \frac{\sin(\theta_{2_1})}{l_p \times \cos\delta \times \sin(\theta_2 - \theta_1)_1} + \frac{\sin(\theta_{2_2})}{l_p \times \cos\delta \times \sin(\theta_2 - \theta_1)_2} + \frac{\sin(\theta_{2_3})}{l_p \times \cos\delta \times \sin(\theta_2 - \theta_1)_3}$$

It can be noted that as the inclination angle of links increases, the horizontal force components become high compared to the conventional manipulator.

c. The rotational stiffness expression about Z axis is derived from the equation 16
The constraints are as follows;
The geometric constraint is (22)

$$L + r_{top} \geq \frac{R_{base}}{2}$$

(22)

The required workspace area should be devoid of Type-I singularities in the workspace. The presence of the three void circles (Type-I singularities) shown in Figure 11 is due to the difference in the projected link lengths $l_p \cos\delta$ and $l_d \cos\delta$. Hence, the maximum reachable workspace is approximated to be a circle with radius R_w. The radius R_w is the distance from the platform centre to the void circle boundary or mutual workspace boundary depending upon whether the void circles are present inside or outside the workspace area (23).

$$R_w \equiv R_{base} - \left(r_{top} + \left| l_p \cos\delta - l_d \cos\delta \right| \right) \geq 100$$

(23)

$$R_w \equiv \left| R_{base} - \left(r_{top} + l_p \cos\delta + l_d \cos\delta \right) \right| \geq 100$$
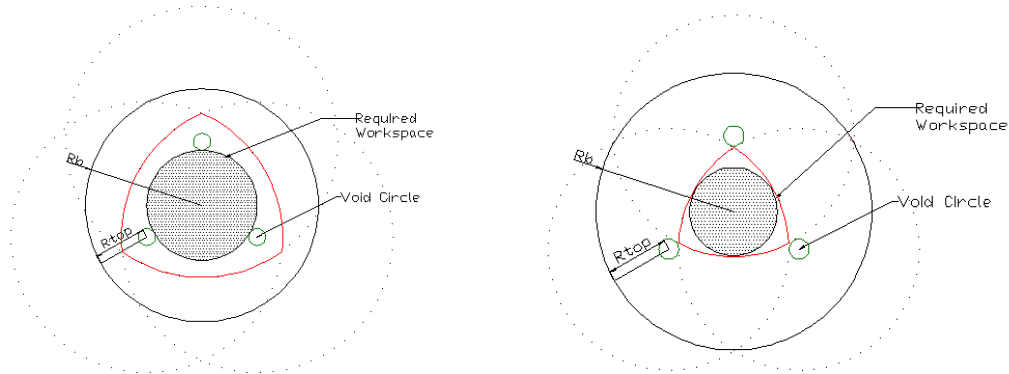
Figure 11. Workspace constraint

Multi-objective Optimization problem statement

The Multi-objective Design Optimization Problem of the model is reinstated as: *To find the optimum design variables X in order to minimize the mass of the mechanism in motion and to maximize its accuracy/stiffness subject to geometric, kinematic and workspace constraints.*
Mathematically, the problem can be summarized as:

minimize $f_1(x)$ = M_{RRR}

maximize $f_2(x)$ = F_{xy} and K_z

Over $\quad X = \begin{bmatrix} l_p & l_d & r_{top} & \delta \end{bmatrix}$ $\qquad$ subject to $\qquad$ $g1: \; L + r_{top} \geq \dfrac{R_{base}}{2}$

$X_{lb} = [100 \;\; 100 \;\; 120 \;\; 0 \;]$ $\qquad\qquad\qquad\qquad$ $g2: \; R_W \geq 100$

$X_{ub} = [200 \;\; 200 \;\; 220 \;\; 70 \;]$

4. RESULTS AND ANALYSIS

Summary of all the parameter modifications are given in Table 2 below. The inclination angle influences the static characteristics which can be inferred by the presence of cosδ term or sinδ term in the expressions.

Table 2 Summary of Modified Expressions

Parameter	Expression
Moment of Inertia	$I_Z = \pi \dfrac{r^4}{4}\left[\left(\dfrac{1}{\cos\delta}\right) + \left(\dfrac{1}{\cos\delta}\right)^3\right]$
Mass moment of Inertia	$I_{ZZ} = \dfrac{MR^2}{4}\left(\dfrac{1}{\sin^2\delta}\right) + \dfrac{ML^2}{3}\left(\sin^2\delta\right)$
Static Force transmission	$f_x = \dfrac{\cos(\theta_{2_1})}{l_p \times \cos\delta \times \sin(\theta_2 - \theta_1)_1} + \dfrac{\cos(\theta_{2_2})}{l_p \times \cos\delta \times \sin(\theta_2 - \theta_1)_2} + \dfrac{\cos(\theta_{2_3})}{l_p \times \cos\delta \times \sin(\theta_2 - \theta_1)_3}$
Inertia Force	$f_{pi} = m_{pi} r_{pi}\begin{bmatrix} \ddot{\theta}_{1i}\sin\theta_{1i} + \dot{\theta}_{1i}^2\cos\theta_{1i} \\ -\ddot{\theta}_{1i}\cos\theta_{1i} + \dot{\theta}_{1i}^2\sin\theta_{1i} \end{bmatrix}$ $\quad where \quad r_{pi} = \left(l_{pi}\cos\delta\right)/2$
Mass in motion	$M_{RRR} = 3 \times \pi r_c^2 \left(l_p + l_d\right)\vartheta$

As discussed in section 3.1, the inertia to bending moment is significantly increased which favors the stiffness of the manipulator. For parallel manipulators high stiffness means high accuracy in positioning. While the mass moment of inertia or rotational inertia is significantly reduced. This might favor the motors while the manipulator is in motion because it can be noticed that the inertia force as shown in Table 2 is also reduced. The inertia force calculation is shown in Appendix B.

4.1. Stiffness Results

The compliance of the entire 3-RRR kinematic chain is calculated using the equation 16 and by taking inverse, the stiffness matrix is obtained. The stiffness matrices are generated for a particular manipulator position and the prototype dimensions are taken for solving the matrices.

The stiffness matrices generated is shown below.

$$e^{+004} \qquad\qquad\qquad\qquad\qquad\qquad\qquad\qquad e^{+005}$$

$$S_\Sigma = \begin{bmatrix} 3.0194 & -0.0329 & -0.0042 \\ -0.0329 & 3.0227 & -0.0060 \\ -0.0042 & -0.0060 & 0.1009 \end{bmatrix}$$

$$S_\Sigma = \begin{bmatrix} 2.0725 & -4.4693 & 3.4513 & -0.1670 & -0.2905 & -0.4882 \\ -4.4693 & 8.3864 & -5.3734 & 0.3644 & 0.5368 & 0.9263 \\ 3.4513 & -5.3734 & 1.7599 & -0.3884 & -0.2331 & -0.5408 \\ -0.1670 & 0.3644 & -0.3884 & 0.0075 & 0.0331 & 0.0433 \\ -0.2905 & 0.5368 & -0.2331 & 0.0331 & 0.0284 & 0.0535 \\ -0.4882 & 0.9263 & -0.5408 & 0.0433 & 0.0535 & 0.1102 \end{bmatrix}$$

Comparing the stiffness matrices above, it is deduced that the modified design yields better stiffness. The last diagonal element in the matrix represents the rotational stiffness component. This component is very less $(0.1009e^{+004})$ for the conventional planar manipulator compared to the modified design $(0.1102e^{+005})$

4.2. Stiffness Mapping

The stiffness values for the entire workspace are generated for the conventional and modified 3-RRR manipulator. The stiffness of the manipulator along the X-Y plane is plotted in Figure 12. For the conventional 3-RRR manipulator and for the modified 3-RRR version, the stiffness values range below 10^5N/m (refer Figure 12a) over a major portion of the workspace. This would increase the accuracy of the manipulator as discussed in [7]. For the modified 3-RRR version, the stiffness value ranges high in the order of 10^6 N/m.
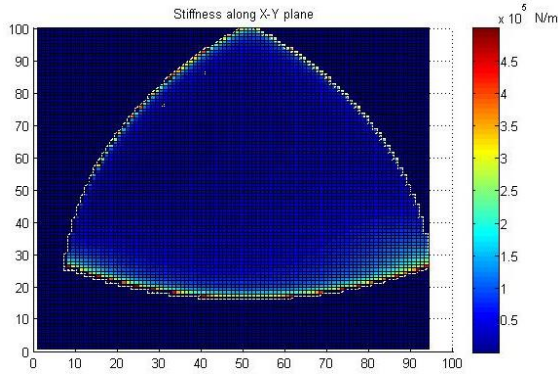
Figure 12a.Stiffness Map in X-Y plane - Conventional 3RRR manipulator
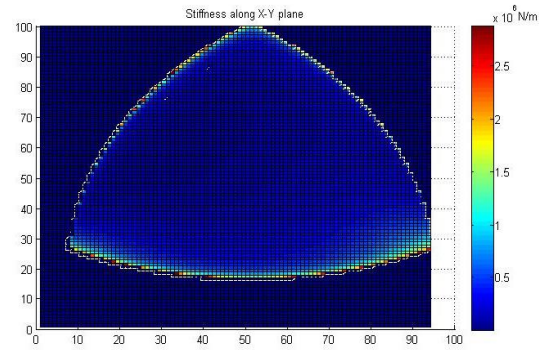
Figure 12b. Stiffness Map in X-Y plane - the Modified 3RRR manipulator

From the results, it is understood that the inclination of the links favors stiffness, force transmission and stress behavior of the links but the inclination angle is to be optimized. This is addressed in the optimization section

4.3. Optimization results

Few selected solutions of the multiobjective statement in sections are shown in Table 3. The solutions shown are the optimized results of the decision variables. The optimized inclination angle δ is found close to 47º.The optimal values obtained for proximal link length are very close to the lower bound values set for the optimization. The reason for this is evident from the force equation 21which has proximal link length in each term of the equation.

It may be noted that, in the optimized results, the difference between the proximal links and the distal links are very large. However the difference between the projected link lengths of the corresponding links will be small and hence the void circles radius is small. It is to be noted that the avoidance of void circle inside the workspace is ensured using the constraint equation 23.

Table 3 The Pareto front solutions for the variables (decision space)

Solutions	Length of proximal links l_p (mm)	Length of distal links l_d (mm)	Radius of Top platform r_{top} (mm)	Inclination angle of link δ (deg)
f_{24}	100	188	120	48.7
f_{25}	100	198	122	47.1
f_{26}	100	180	127	47.7
f_{27}	100	198	122	47.1

4.4 Application of non-planar spatial links

Generally, planar mechanisms have limitations in payload capacity and they find their applications in machining, MEMS and other applications where light load is preferrable. The non- planar links gives scope for using planar mechanisms with high payload. For example one such application is the 6-DOF shake table developed by the authors for simulating the earthquake data.
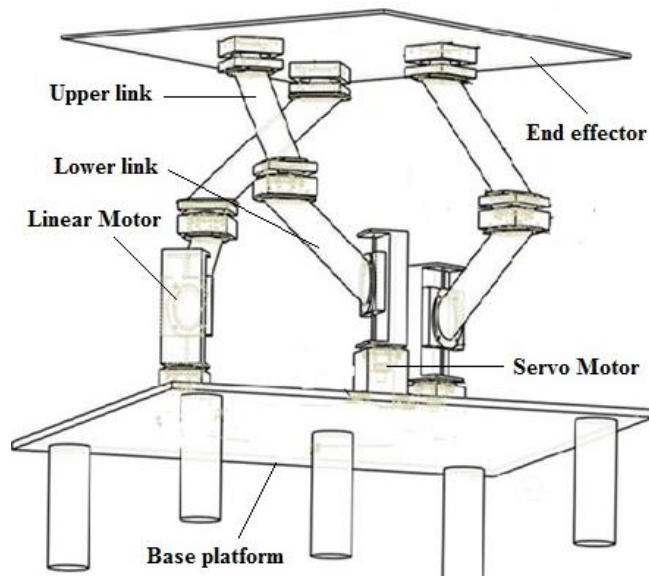
Figure 13. A 3D model of 6-DOF Shake Table based on 3-legged RPRS topology

5. CONCLUSION

In this paper non-planar links are proposed for a class of planar parallel manipulators by which the distance between the mobile platform and base platform is raised. NPL Arrangement is implemented with the expectation of increasing the payload capacity, and decreasing the cantilever nature of the links. This is supported by the improvement in the static characteristics behavior of non-planar links.

The following specific conclusions can be drawn:
   a. The formulated inertia tensor for the modified links substantiates **the improvement of stiffness and dynamics** of the modified links of legs.
   b. **The stiffness values along all the three principal directions** for the modified 3-RRR manipulator are high in comparison with conventional manipulator.
   c. Stiffness in particular, is also mapped onto the entire constant orientation workspace and the results are 10 times better compared with the conventional planar parallel manipulator.
   d. **Low inertia force characterizes the dynamic model** of the legs for 3-RRR manipulator.

As, the inclination angle affects the workspace area,it is essential to determine the optimal inclination angle which will optimize force transmission, stiffness and mass in motion while fulfilling the workspace area requirement.

ACKNOWLEDGEMENTS

REFERENCES
[1] J.-P. Merlet, C.M. Gosselin, N. Mouly, "Workspace of planar parallel manipulators", Mechanism and Machine Theory, 33 (1–2) (1998), pp. 7–20.
[2] C.M. Gosselin, J. Martin, "Determination of the workspace of planar parallel manipulators with joint limits", *Robotics and Autonomous Systems* 17 (3), (1996), pp. 129–138.
[3] J.P. Merlet, "Direct kinematics of planar parallel manipulators", *Proceedings of IEEE International Conference on Robotics and Automation*, 4(1996), pp. 3744–3749.
[4] Bonev, I. A., and Gosselin, C. M., "Singularity Loci of Planar Parallel Manipulators with Revolute Joints", *Proc. 2nd Workshop on Computational Kinematics*, Seoul, (2001), pp. 291–299
[5] M.H.R. Daniali, J. Angeles, Singularity analysis of planar parallel manipulators, *Mechanism and Machine Theory,* 30 (5), (1995), pp.665–678.

[6] C.M. Gosselin and J. Angeles, "The optimal kinematic design of a planar three-degree-of-freedom parallel manipulator", *J Mech Transmission and Automation* 110 (3) (1988), pp. 35–41.

[7] D. Chablat, S. Caro, R. Ur-Rehman, P. Wenger, "Comparison of Planar Parallel Manipulator Architectures based on a Multi-objective Design Optimization Approach", *ASME International Design Engineering Technical Conferences and Computers and Information in Engineering Conference* (2010): pp. 861-870.

[8] Clement, Gosselin. "Stiffness Mapping for Parallel Manipulators", *IEEE Transactions on Robotics and Automation*, 6(3): (1990), pp. 377-382.

[9] Kim, Whee-kuk, Byung-Ju Yi, and Whang Cho. "RCC characteristics of planar/spherical 3-DOF parallel mechanisms with joint compliances". *Journal of Mechanical Design,* 122, no. 1 (2000), pp. 10-16.

[10] Kang. B, Chu. J and Mills, J.K, "Design of high speed planar parallel manipulator and multiple simultaneous specification control", In *Robotics and Automation, Proceedings 2001 ICRA. IEEE International Conference on*, vol. 3,(2001), pp. 2723-2728.

[11] Chang, W.T., Lin, C.C. and Lee, J.-J., "Force Transmissibility Performance of Parallel Manipulators", *Journal of Robotic Systems*, 20 (2003), pp.659–670.

[12] Klimchik A., Pashkevich A., Caro S., and Chablat D. "Stiffness matrix of manipulators with passive joints: computational aspects", *IEEE Transactions on Robotics,* 28(4), (2011), pp. 955 – 958.

[13] El-Khasawneh, Bashar S., and P M. Ferreira. "Computation of stiffness and stiffness bounds for parallel link manipulators". *International Journal of Machine Tools and Manufacture* 39, no. 2 (1999): pp. 321-342.

[14] Pashkevich, Anatoly, Philippe Wenger, and Damien Chablat. "Kinematic and stiffness analysis of the Orthoglide, a PKM with simple, regular workspace and homogeneous performances". In *Robotics and Automation, 2007 IEEE International Conference on*, (2007), pp. 549-554.

[15] G. Yang, W. Chen, and I-M.Chen, "A Geometrical method for the Singularity Analysis of 3-RRR planar parallel robots with different actuation schemes", *In proceedings of IEEE/RSJ International Conference on Intelligent Robots and Systems (IROS'01),(* 2002), pp. 2055-2060.

[16] Firmani, Flavio, and Ron P. Podhorodeski. "Singularity analysis of planar parallel manipulators based on forward kinematic solutions." *Mechanism and Machine Theory* 44, no. 7 (2009): 1386-1399.

[17] Kiyoshi Nagai and Zhengyong Liu, "A systematic approach to stiffness analysis of parallel mechanisms", *In Robotics and Automation, ICRA 2008. IEEE International Conference on*, (2008) pp. 1543-1548.

[18] Jorge Angeles, "On Twist and Wrench Generators and Annihilators". *Computer-Aided Analysis of Rigid and Flexible Mechanical Systems* McGill University, Canada, *NATO ASI Series*, 268(1994), pp 379-411.

[19] Vyas A., Vasudevan S., Ganesh M., Dash A.K., **"**Fabrication and control of 3-DOF RRR planar parallel manipulators with non-planar links", *International Journal of Applied Engineering Research*, (2014).

[20] Tsai, L.W., *Robot analysis: the mechanics of serial and parallel manipulators*. John Wiley & Sons, 1999.

Appendix A : Notations used in stiffness modeling

J_{mn} denotes the nth joint of mth leg.

$_T C$ denotes the transformed compliance

$_T C^{Lmn}$ denotes the transformed link compliance for n^{th} link of mth leg.

C^{Jmn} denotes the joint compliance for n^{th} joint of mth leg.

C^{Cmn} denotes the cumulative compliance (m^{th} joint and m^{-1th} transformed link together)

$_T C^{Cmn}$ denotes the transformed cumulative compliance for n^{th} joint of mth leg.

$C_{1\Sigma}$ denotes the total compliance of mth leg (all the links and joints together)

Appendix B Inertia Force Computation

The inertia force and moment of links about its mass center is determined by Newton Euler formulation. Then the modified inertia values are employed in the moment calculations.
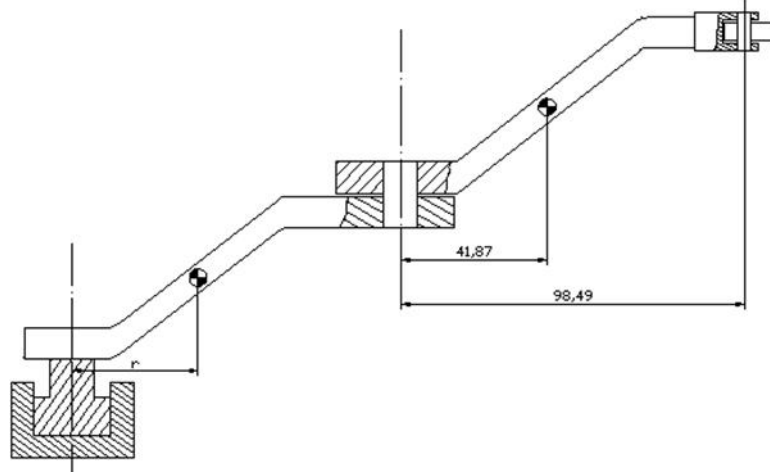
The acceleration of the link is determined for link's centre of mass. It is done by taking the second derivative of the position vector of links centre of mass. The position vector of p_i is given below

$$P_{pi} = \begin{bmatrix} O_{x_i} + r_{pi}\cos\theta_{1i} \\ O_{y_i} + r_{pi}\sin\theta_{1i} \end{bmatrix} \tag{B1}$$

The second derivative of the equation 20, with respect to time yields

$$a_{pi} = \frac{d}{dt}\left(\frac{d}{dt}\begin{bmatrix} O_{x_i} + r_{pi}\cos\theta_{1i} \\ O_{y_i} + r_{pi}\sin\theta_{1i} \end{bmatrix}\right)$$
$$= r_{pi}\begin{bmatrix} -\ddot{\theta}_{1i}\sin\theta_{1i} + \dot{\theta}_{1i}^2\cos\theta_{1i} \\ \ddot{\theta}_{1i}\cos\theta_{1i} - \dot{\theta}_{1i}^2\sin\theta_{1i} \end{bmatrix} \text{ where } r_{pi} = \left(l_{pi}\cos\delta\right)/2 \tag{B2}$$

The inertia force of the mass of first link is determined as

$$f_{pi} = -m_{pi}\left(a_{pi} - g\right) \tag{B3}$$

The moment of the link about the pivotal point p_i is given as

$$M_{pi} = \ddot{\theta}_{1i}I_{pi}$$
$$\text{where } I_{pi} = I_{ZZ} = \frac{MR^2}{4}\left(\frac{1}{\sin^2\delta}\right) + \frac{ML^2}{3}\left(\sin^2\delta\right) \tag{B4}$$

The new inertia value obtained in equation 6 is substituted in the equation B4. It can be observed that the inertia force and the moment of the link are considerably reduced with the usage of non-planar links. Similarly, the above procedure can be repeated for the inertia force f_{di} at d_i and the moment M_{di} about d_i. Having estimated the inertia forces and moments of the links, the actuator torques can be obtained by using the principle of virtual work $\tau_i = -J_m^{-T}\left(\sum F_i\right)$